AEDC-TR-74-32

Cy. 1

ARGON CONDENSATION IN FREE-JET EXPANSIONS

J. W. L. Lewis and W. D. Williams
ARO, Inc.

VON KÁRMÁN GAS DYNAMICS FACILITY
ARNOLD ENGINEERING DEVELOPMENT CENTER
AIR FORCE SYSTEMS COMMAND
ARNOLD AIR FORCE STATION, TENNESSEE 37389

July 1974

Final Report for Period November 1, 1972 — July 31, 1973

Approved for public release; distribution unlimited.

Prepared for

ARNOLD ENGINEERING DEVELOPMENT CENTER (DYFS)
ARNOLD AIR FORCE STATION, TN 37389

NOTICES

When U. S. Government drawings specifications, or other data are used for any purpose other than a definitely related Government procurement operation, the Government thereby incurs no responsibility nor any obligation whatsoever, and the fact that the Government may have formulated, furnished, or in any way supplied the said drawings, specifications, or other data, is not to be regarded by implication or otherwise, or in any manner licensing the holder or any other person or corporation, or conveying any rights or permission to manufacture, use, or sell any patented invention that may in any way be related thereto.

Qualified users may obtain copies of this report from the Defense Documentation Center.

References to named commercial products in this report are not to be considered in any sense as an endorsement of the product by the United States Air Force or the Government.

APPROVAL STATEMENT

This technical report has been reviewed and is approved.

Eules L. Hively

EULES L. HIVELY
Research and Development Division
Directorate of Technology

Robert O Dietz

ROBERT O. DIETZ
Director of Technology

UNCLASSIFIED

SECURITY CLASSIFICATION OF THIS PAGE (When Data Entered)

REPORT DOCUMENTATION PAGE		READ INSTRUCTIONS BEFORE COMPLETING FORM
1. REPORT NUMBER AEDC-TR-74-32	2. GOVT ACCESSION NO.	3. RECIPIENT'S CATALOG NUMBER
4. TITLE (and Subtitle) ARGON CONDENSATION IN FREE-JET EXPANSIONS		5. TYPE OF REPORT & PERIOD COVERED Final Report - November 1, 1972 - July 31, 1973 6. PERFORMING ORG. REPORT NUMBER
7. AUTHOR(s) J. W. L. Lewis and W. D. Williams, ARO, Inc.		8. CONTRACT OR GRANT NUMBER(s)
9. PERFORMING ORGANIZATION NAME AND ADDRESS Arnold Engineering Development Center Arnold Air Force Station, Tennessee 37389		10. PROGRAM ELEMENT, PROJECT, TASK AREA & WORK UNIT NUMBERS Program Element 65802F
11. CONTROLLING OFFICE NAME AND ADDRESS Arnold Engineering Development Center (DYFS) Arnold Air Force Station, TN 37389		12. REPORT DATE July 1974 13. NUMBER OF PAGES 38
14. MONITORING AGENCY NAME & ADDRESS(if different from Controlling Office)		15. SECURITY CLASS. (of this report) UNCLASSIFIED 15a. DECLASSIFICATION/DOWNGRADING SCHEDULE N/A

16. DISTRIBUTION STATEMENT (of this Report)

Approved for public release; distribution unlimited.

17. DISTRIBUTION STATEMENT (of the abstract entered in Block 20, if different from Report)

18. SUPPLEMENTARY NOTES

Available in DDC.

19. KEY WORDS (Continue on reverse side if necessary and identify by block number)

argon
condensation
expansion
depolarization
laser
Rayleigh scattering
supersaturation

20. ABSTRACT (Continue on reverse side if necessary and identify by block number)

Homogeneous condensation of argon was observed using sonic orifice expansion flow fields. The room temperature argon was studied over the range of reservoir pressures from 200 to 750 torr using a 3.2-mm orifice diameter. Condensation onset and the subsequent cluster growth was observed using laser Rayleigh scattering, and maximum supersaturation ratios as a function of reservoir pressures were determined. Depolarization ratio

DD FORM 1 JAN 73 1473 EDITION OF 1 NOV 65 IS OBSOLETE

UNCLASSIFIED

SECURITY CLASSIFICATION OF THIS PAGE (When Data Entered)

20. Continued.

measurements were performed for the 750-torr expansion, and shape changes of the cluster were observed throughout the growth region. Comparisons of these results and previous mass spectrometric data are made, and specifically the mass fraction of argon condensate and cluster sizes are estimated.

AFSC
Arnold AFS Tenn

PREFACE

The work reported herein was conducted at the Arnold Engineering Development Center (AEDC), Air Force Systems Command (AFSC), under the sponsorship of Air Force Cambridge Research Laboratories (AFCRL), AFSC, under Program Element 65802F. The AFCRL project monitor was R. E. Good, who provided the technical objectives of the project. The results were obtained by ARO, Inc. (a subsidiary of Sverdrup & Parcel and Associates, Inc.), contract operator of AEDC, AFSC, Arnold Air Force Station, Tennessee. This work was conducted from November 1972 to July 1973 under ARO Project No. VF233, and the manuscript (ARO Control No. ARO-VKF-TR-74-13) was submitted for publication on January 18, 1974.

CONTENTS

ILLUSTRATIONS

TABLES

1.0 INTRODUCTION AND THEORY

1.1 INTRODUCTION

Interest in the understanding of the fluid mechanics and rate kinetics of two-phase flow fields results not only from a desire to exploit such flows for the study of dimer and cluster collision processes, but also from a preference for avoiding their occurrence by judicious selection of the reservoir parameters, if possible. In the latter category are included aerospace simulation facilities, where such processes affect the aerodynamic simulation parameters, and fluid mechanical devices, such as turbines, which suffer loss in efficiency as a result of condensation. The authors' interest in condensing supersonic and hypersonic flow fields arises from a desire to characterize further the cluster growth process resulting from homogeneous condensation for the purpose of understanding both the dissimilar areas of chemical kinetics in two-phase flows and enhanced scattering by the clusters of radiation incident upon a condensed flow field.

Several previous studies of condensation in expanding gas flows have considered the cluster growth of argon (Ar) because it is a nontoxic, nonreactive, inexpensive, noble gas atom which is believed to be capable of description using a spherically symmetric Lennard-Jones 12-6 interatomic potential. Such spherical symmetry greatly simplifies theoretical calculations of equilibrium Ar_2 dimer concentrations, the values of which are required for rate calculations. Additionally, the absence of internal, ground electronic state modes of motion precludes the existence of relaxation phenomena in the flow field and enables the accurate prediction of gas dynamic properties throughout the flow field. Finally, and of prime importance, Ar condenses readily. The majority of these previous studies (Refs. 1 and 2) have relied on mass spectrometric detection of the clusters, or polymers, and despite the inherent difficulties of the uncertainty of ionization cross sections and diffusive separation effects, this method of measurement has definitively indicated the onset of condensation. It should be noted that such detection methods, although not all alike in sampling procedures, have the common feature of being located far from both the flow source and the point of condensation onset. As a result, the detected polymer signals are the result of integration of the rate equations along the streamtube of the flow through normally large gradients of both temperature and density, a most undesirable effect. Consequently, one must resort to assuming various kinetic models, performing the required integrations and comparing the result with the experimental values (Ref. 3).

Recently, electron diffraction studies (Ref. 4) have been performed on argon cluster beams, and, although these measurements have indicated the existence of large clusters, quantitative estimates of the concentration of the clusters have not been possible. It should be noted that the experimental configuration of observing a sampled, or skimmed, beam is used for such diffraction studies just as it is for mass spectrometric detection; consequently, considerations concerning the observation of an integrated effect apply equally to the diffraction method of observation so long as collisionless sampling methods are employed. The work of Audit (Ref. 4) has demonstrated the utility of the technique for distinguishing between liquid and solid phase condensation by observation of the diffraction pattern and the spatial extent of ordering present. Moreover, estimates of interatomic spacing and temperature of the crystalline structure are both possible, and this information is most useful for determining the partition of enthalpy between the condensate and gas phases of the flow field. Recently, measurements (Ref. 5) of the monomer flow speed using mass spectrometric methods have enabled the final mass fraction of condensate to be determined, and the electron beam fluorescence method (Ref. 6) has been applied to the task of determining condensate mass fractions for the far field, low-density region of nitrogen (N_2) condensing flows. Moreover, Rayleigh scattering measurements (Ref. 6) are capable of determining within the flow field the spatial location of condensation onset as well as following the cluster growth process. Additionally, in the early stages of cluster growth when only dimers exist, quantitative estimates of dimer mole fraction are provided by such measurements. This information, of course, provides a rather stringent test for condensation theories, and the test itself does not suffer such possible ambiguities as sampling perturbations and cluster dissociation by electron impact as does the test of the mass spectrometer.

Historically, the observation of dimers of Ar in a sampled, molecular flow by Leckenby and Robbins (Ref. 7) signaled the beginning of recent intensive investigations of expansion flow fields by Golomb, et al. (Refs. 1 and 2), Hagena and coworkers (Ref. 8 and 9), and Milne et al. (Ref. 3). It should be noted that the authors in Refs. 1 through 3 all used conventional quadrupole or magnetic sector mass spectrometers for the far-field detection, whereas Hagena employed a specially constructed retarding field device capable of determining a quantity resembling the mean value of N/Z, the ratio of number of atoms per cluster and the charge of the cluster.

Since the primary interest at present is in the nonequilibrium production of condensate in expansion flows, the notable work of Leckenby and Robbins is of importance to this work only for historical purposes, and attention to previous work will be directed to that of Refs. 1 and 2 as well as the most recent work of Yealland et al. (Ref. 10). It is interesting to note the varying degrees of confidence by these investigators in quantitative interpretation of their respective data. The work of Golomb et al. (Ref. 2) is noteworthy for attention to the problems and ambiguities arising from the sampling process itself, which occur in density regions commonly considered as free molecular. Definite differences in results are noted, for example, whether the skimmer is cooled or uncooled and whether the mass spectrometer extracts the ions either parallel or perpendicular to the flow velocity. In light of such differences, Golomb et al. do not place great reliance upon the absolute values of their results but do contend that the onset of massive condensation is observed. In addition to observation of the increasing concentration of polymers in the sampled flow, the study of Golomb et al. also considered variations in measured flow speed with pressure as an indication of condensation onset, and Bailey (Ref. 5) has determined the mass fraction of condensate of various species using this technique.

An opposing view of the confidence to be given quantitative interpretation of mass spectrometric data is obviously held by Milne et al. who go so far as to use their results to attempt to determine the functional dependence of the various rate constants. With similar, but lesser, fervency, Yealland et al. present quantitative functions for the prediction of dimer mole fractions for the expansion flow fields they investigated. Hagena asserts his results are quantitatively accurate to the extent that he can characterize the expansion by some type of mean value of cluster size. Finally, authors in both Refs. 2 and 8 have considered in detail the scaling of condensation onset or cluster size with orifice diameter, reservoir pressure, temperature, and gas specie.

A serious difficulty encountered in comparing results of these investigations is the necessity of extrapolating various parameters based upon the experimentally determined scaling laws. Although such an extrapolation is questionable and undesirable, no other choice exists. As will be discussed in detail in a later section, such a comparison of the results of Refs. 2 and 8 does not yield agreement. For example, for reservoir pressures, P_o, for which Golomb et al. observed a preponderance of dimers of Ar_2, Hagena and Obert predict the mean cluster size to be 20. The mean cluster size of Ar, $(N/Z)^*$, scales with orifice diameter, D, as $P_o D^{0.8}$ according to Ref. 8, whereas the dimer

peak of Ref. 2 scales essentially as $P_o D^{0.5}$, and the situation is no better with regard to scaling laws relating P_o and reservoir temperature, T_o. The purpose of this work was to obtain information concerning the spatial location of condensation onset, supersaturation ratios as a function of reservoir pressure, and cluster growth processes, including estimates, if possible, of the size of the scattering cluster.

1.2 RAYLEIGH SCATTERING

Since thorough discussions of photon-atom and molecule scattering processes have been presented elsewhere (Ref. 11), only a brief review of the phenomenon will be considered here. Attention will be restricted to photon-molecule scattering processes for which no change in internal energy states exists, and this process will be designated as Rayleigh scattering. The laser source of intensity, I_o, and wavelength, λ, provides a photon beam perpendicular to both the gas flow velocity and the unit vector in the direction of the collection optics for the scattered radiation. Figure 1 shows this configuration as well as the polarization

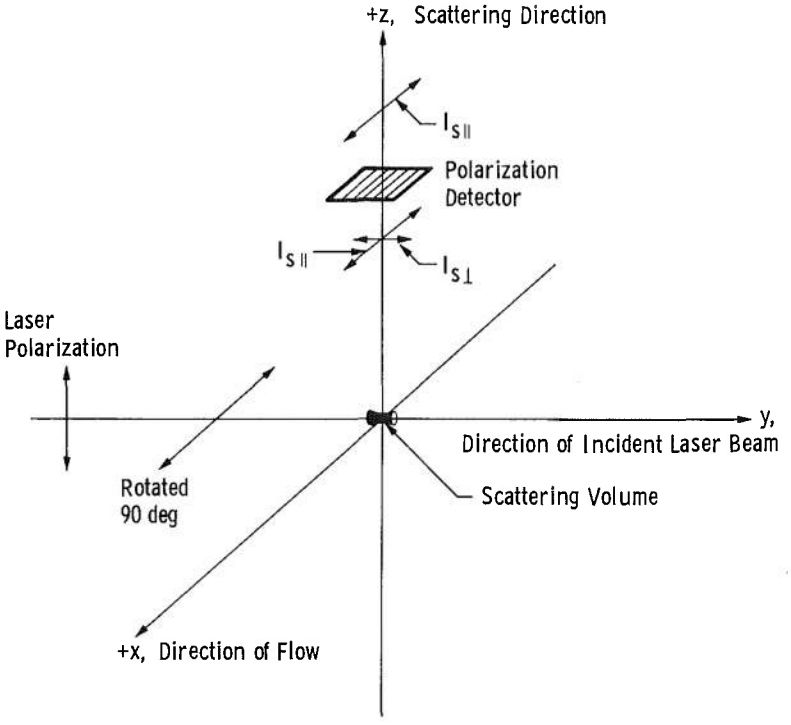

Figure 1. Experimental configuration.

vectors of the incident and scattered radiation. It is known that intensity, I_S, with wavelength, λ, scattered from a collection of uniform scattering sources of number density, N, is given by

$$I_s/I_o = K_\alpha N\alpha^2/\lambda^4 \tag{1}$$

where K_α includes various transmission and optical sensitivity constants as well as fundamental atomic constants and α is the polarizability of the scatterer.

The polarizability of the monomer Ar is known (Ref. 11) to be 1.64 $\mathring{A}^3$. Since spinless, ground-state Ar atoms of spherical symmetry will be considered, the depolarization ratio is zero for gas densities sufficiently low that insignificant numbers of quasi-molecules Ar_2 exist.

Following onset of condensation, a collection of clusters or polymers of various sizes exist within the flow, and the number density of the j-mer of the collection, i.e., Ar_j, is denoted by N_j; the polarizability of the j-mer is designated as α_j. The scattering equation for such an assembly is given by

$$I_s/I_o = (K_\alpha/\lambda^4) \times \sum_{i=1}^{\infty} N_i\alpha_i^2 \tag{2}$$

or

$$I_s/I_o = (K_\alpha/\lambda^4)N_T\alpha_1^2\left[\left(\frac{N_1}{N_T}\right) + \sum_{i=2}^{\infty}(N_i/N_T)(\alpha_i/\alpha_1)^2\right] \tag{3}$$

where

$$N_T = \sum_{i=1}^{\infty} N_i$$

Using the reservoir number density for nondimensionalizing the important parts of the equations,

$$I_s/I_o = (K_\alpha N_o\alpha_1^2/\lambda^4) \times (N_T/N_o) \times \left[\left(\frac{N_1}{N_T}\right) + \sum_{i=2}^{\infty}\frac{(N_i/N_o)}{(N_T/N_o)} \times (\alpha_i/\alpha_1)^2\right] \tag{4}$$

For isentropic, noncondensing expansions of the monomer from the same reservoir density, N_o, Eq. (4) would be

$$(I_s/I_o)^o = (K_a N_o \alpha_1^2/\lambda^4)(N_1/N_o)^o \tag{5}$$

where the form of $(N_1/N_o)^o$ is known (Ref. 12) as a function of axial distance, x/D, and specific heat ratio, γ.

The ratio of Eq. (4) and (5) yields

$$[(I_s/I_o)/(I_s/I_o)^o] - (N_1/N_1^o) = (N_T/N_1^o) \times X_c \times \sum_{i=2}^{\infty} p(i)(\alpha_i/\alpha_1)^2 \tag{6}$$

where the mole fraction of condensate, X_c, is defined as

$$X_c = \sum_{i=2}^{\infty} N_i/N_T = N_c/N_T \tag{7}$$

and the probability of the existence of an i-mer p(i) is defined as

$$p(i) = N_i \Big/ \sum_{i=2}^{\infty} N_i \tag{8}$$

The condensate mass fraction, g, is defined as

$$g = \sum_{i=2}^{\infty} i(N_i/N_T) \Big/ \sum_{i=1}^{\infty} i(N_i/N_T) \tag{9}$$

or

$$g = (N_c/N_T) \times \sum_{i=2}^{\infty} p(i) \times i/[(N_1/N_T) + (N_c/N_T) \sum_{i=2}^{\infty} i\,p(i)] \tag{10}$$

For the purpose of data interpretation and comparisons, Eqs. (6) and (10) will be specialized to the following three cases:

1. The cluster distribution is characterized by a Dirac delta function such that all clusters are dimers, and the mole fraction of condensate is much less than unity,
2. The cluster distribution is characterized by a Dirac delta function such that all clusters are J-mers, where J >> 1, and the mole fraction of condensate is much less than unity,, and
3. The cluster distribution is characterized by a Poisson distribution function with mean cluster size of J >> 1.

For the first case, since the mole fraction of condensate $X_c \ll 1$,

$$N_1^\circ \approx N_1 \approx N_T$$

so Eqs. (6) and (10) become

$$R = X_2 \times (a_2/a_1)^2 \tag{11}$$

and

$$g = 2X_2/(1 + X_2) \tag{12}$$

where X_i is the mole fraction of the i-mer and

$$R = (I_s/I_o)/(I_s/I_o)^\circ - 1$$

Since the Ar_2 dimer is a weakly bound, van der Waals-type molecule, it is reasonable to assume (Ref. 11)

$$a_2/a_1 \approx 2$$

Therefore,

$$R \approx 4X_2 \tag{13}$$

Consequently, for expansion flow fields for which $g \ll 1$ and only dimers exist throughout the flow field, a measurement of the scattering function R provides a direct measure of X_2 by means of Eq. (13), and, of course, g is determined using X_2 and Eq. (12). Although the reservoir conditions may be such as to produce a flow field containing sufficient condensate in the far field to invalidate the assumptions of Case 1, a region remains in the spatial vicinity of condensation onset for which the assumptions of Case 1 are valid. Intuitively, one expects such a region of validity to become more narrow in spatial extent as the reservoir conditions are altered in the direction of enhancement of condensation.

Considering Case 2 for which p(i) equals unity for i = J and zero otherwise and $X_c \ll 1$, Eq. (6) becomes

$$R \approx X_c(a_J/a_1)^2 \tag{14}$$

where it is assumed that

$$N_1^\circ \approx N_1 \approx N_T$$

If it is assumed that

$$\alpha_J/\alpha_1 \approx J$$

Eq. (14) becomes

$$R \approx J^2 X_c \tag{15}$$

It should be noted this approximation regarding the polarizability of the j-mer, $J >> 1$, becomes invalid when long-range order or collective effects are significant. The upper limit in J for which this approximation is valid is not known at present. The mass fraction of condensate is given by

$$g = JX_c/[1 + (J - 1)X_c] \tag{16}$$

Considering Case 3 for which the distribution function is characterized by a Poisson distribution of mean cluster size of J

$$p(i) = e^{-J} J^i/i! \tag{17}$$

It is assumed that only the clusters are described by such a distribution; the monomer is not included. As will be shown later, the distributions to be considered will be such that the mean cluster size J will greatly exceed unity and the contribution to the usual Poisson distribution by p(1) is negligible. That is to say, because of the large values of J, the normalization of the Poisson distribution function is not significantly affected by our neglect of p(1).

As a first approximation, it is assumed that N_1/N_1° and N_T/N_1° are approximately unity, so Eq. (6) is written as

$$R = X_c \sum_{i=2}^{\infty} p(i)(\alpha_i/\alpha_1)^2 \tag{18}$$

where p(i) is given by Eq. (17). Concerning the approximation

$$N_1/N_1^\circ \approx 1$$

if such is not the case it is probable, and experimentally observed, that

$$(I_s/I_o)/(I_s/I_o)^\circ >> 1$$

so that little error is encountered on the left-hand side of Eq. (6) by assuming $N_1 \approx N_1^o$. The primary error is expected to arise on the right-hand side of Eq. (6) in approximating N_T by N_1^o. However, it is suggested that any error introduced by such an approximation is perhaps insignificant for the flow fields investigated in this study.

Once again approximating α_i/α_1 by i, it is seen that the second moment of the Poisson distribution is required for the evaluation of R in Eq. (18). It is easily shown that

$$\sum_{i=2}^{\infty} i^2 p(i) = J^2 + J$$

where

$$J = \sum_{i=2}^{\infty} i\,p(i)$$

and is the mean cluster size of the distribution. Therefore,

$$R \approx X_c(J^2 + J) \tag{19}$$

and g is given by

$$g = X_c J/[1 + X_c(J - 1)] \tag{20}$$

or for $J \gg 1$

$$g = X_c J/(1 + X_c J). \tag{21}$$

The approach taken for the analysis of the experimental results will be to obtain experimental values of R, use the results of Ref. 8 for values of J, calculate X_c and g, and compare these results with those of Golomb et al. (Ref. 2) and Bailey (Ref. 5).

Finally, it should be noted that measurement of the depolarization ratio, ρ, through the cluster growth region provides an interesting account of the change of spatial symmetry of the scatterer. In the event of scattering by only monomers, ρ of Ar is zero. As the cluster growth proceeds through the dimer and trimer stages, one would intuitively expect a reduction in degree of symmetry and an increase from zero of the depolarization ratio. As the cluster grows and assumes larger dimensions, it is expected that the degree of symmetry should once again increase and ρ should decrease. Consequently, a qualitative picture of the growth process will result.

2.0 EXPERIMENTAL APPARATUS AND METHOD

2.1 GAS SOURCE AND VACUUM CHAMBER

Since the experimental apparatus is essentially the same as that described in Ref. 6, only a brief summary of the system will be presented.

The sonic orifice source was of 3.2-mm diameter with a diameter-to-thickness ratio of approximately 25. The orifice was located at the end of a tubular stainless steel reservoir of 1-cm inner diameter, and equilibration of the gas and tube wall temperatures was assured. Reservoir temperature and pressure were measured using calibrated transducers, and the flow-field data were acquired using argon of both high and ultrahigh purity, the latter being 99.999 percent pure, and no difference in the results was noted. Two 0.025-μm particulate filters were installed in the inlet gas line to minimize heterogeneous condensation processes. The gas source was mounted on a traversing mechanism to provide three degrees of freedom and enable flow-field profile measurements with fixed optical instrumentation. The movement mechanism has an accuracy and reproducibility of 0.013 cm in the axial direction, and a more detailed description and sketches are given in Ref. 6.

The vacuum chamber enclosing the motor-driven traversing mechanism was cryopumped using liquid N_2 and gaseous helium (He), and background pressures of 10^{-7} and less than 10^{-5} torr were attained for no gas flow and maximum mass flow rate, respectively. Pressure and temperature fluctuations in the reservoir were on the order of one to two percent in the worst case and typically were much smaller. A more complete description of both the gas dynamic instrumentation and chamber systems is found in Ref. 6.

2.2 RAYLEIGH SCATTERING APPARATUS

Figure 1 shows the experimental configuration employed for the laser scattering studies. A Coherent Radiation Laboratories Model 52-B argon ion laser was used with incident wavelength set at 4880 Å and a 0.5-watt intensity. A half-wave plate was used on the input beam to rotate the polarization vector by 90 deg, and HN-22 Polaroid® material was inserted in the detection train to select either the parallel or perpendicular polarization component of the scattered radiation. The

rejection ratio for transmission of crossed polarization vector intensity was 10^5. Details of the optical apertures used to reduce background scattering are presented in Ref. 6 and will not be repeated here. An International Telephone and Telegraph (ITT) FW130 photomultiplier tube cooled to -26°C was used for the photon counting detection method. For pulse processing and registration, an Ortec system consisting of amplifier, discriminator, and either a dual counter/timer or a rate-meter was utilized. Spectral isolation was accomplished by means of a 10-Å half-width transmission filter centered at 4880 Å, the transmission curve of which is shown in Fig. 2. The sample volume was on the order of 1 mm^3. Linearity of the output signal with incident laser power was verified. The pressure variation of the Rayleigh scattered radiation from Ar has been measured over three orders of magnitude range in pressure, and linearity has been observed. Finally, room temperature measurements of the depolarization ratio of Ar were performed for several pressures and it was found that $\rho \lesssim 1 \times 10^{-4}$.

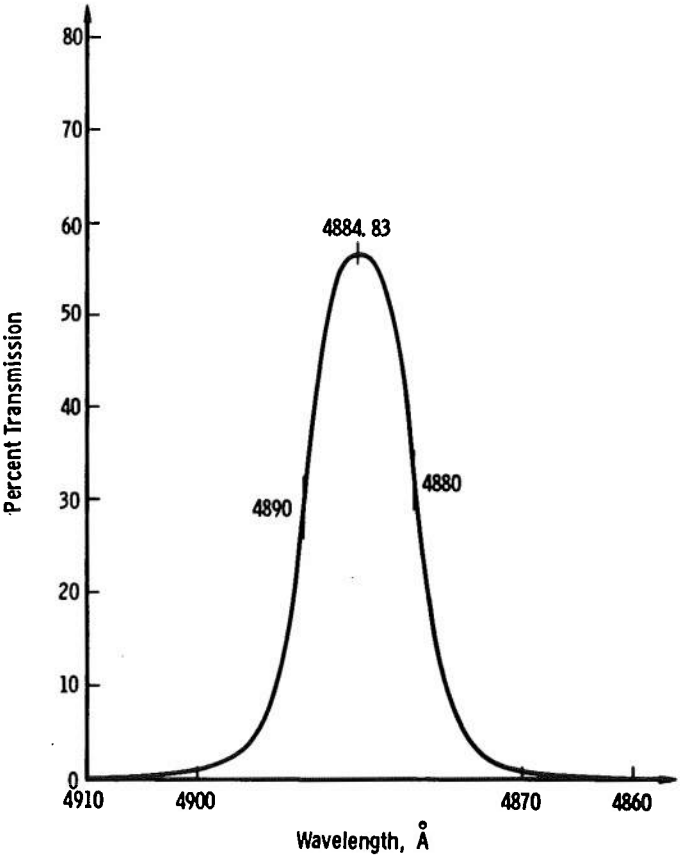

Figure 2. Filter transmission curve.

The procedure for alignment of the laser beam with respect to the gas source in the axial direction was accomplished using a pitot probe of fixed location within the chamber, and Ref. 6 describes this procedure. The centerline of the flow was found using radial profiles and selecting the center of symmetry. Such profile measurements were required for several axial positions to define the direction of the axis of the cylindrically symmetrical flow field.

Although calibrations of the constant K_α in Eq. (1) were performed using room-temperature, static Ar gas of known density and polarizability, a method of calibration or normalization was employed during the course of the measurements which obviated corrections caused by position changes of the traversing mechanism of the source incurred by the cooling of the mechanism from room temperature to its much lower steady-state value. This procedure is mentioned in a following section.

The photomultiplier tube dark count rate, determined with the laser source off, and the background count rate, determined with no gas within the scattering volume, were assumed to be additive corrections and were simply subtracted from the experimental photon count rate values.

3.0 EXPERIMENTAL RESULTS AND ANALYSIS

3.1 RESULTS

Sonic orifice expansion flow fields with reservoir pressures of 200, 250, 350, 500, and 750 torr were produced, and Rayleigh scattering measurements were performed over the axial distance range of $0.4 \lesssim x/D \lesssim 25$. The reservoir temperature employed was constant for each value of P_o but varied from 275°K at 250 torr to 281°K for P_o = 500 torr, and the data are reported for the nominal reservoir temperature of 280°K. Using the isentropic flow predictions of Sherman and Ashkenas (Ref. 12), Fig. 3 shows the expansion isentropes plotted in the P-T plane, and also shown is the vapor pressure curve of bulk Ar as given by Ref. 13. The crossing of the vapor pressure curve by the various isentropes approximately defines the values of P, T and, thereby, x/D of the flow field for which saturation occurs. Continuation of the expansion along the isentrope, once having crossed the vapor pressure curve, constitutes a supersaturated flow field for which condensation onset may occur.

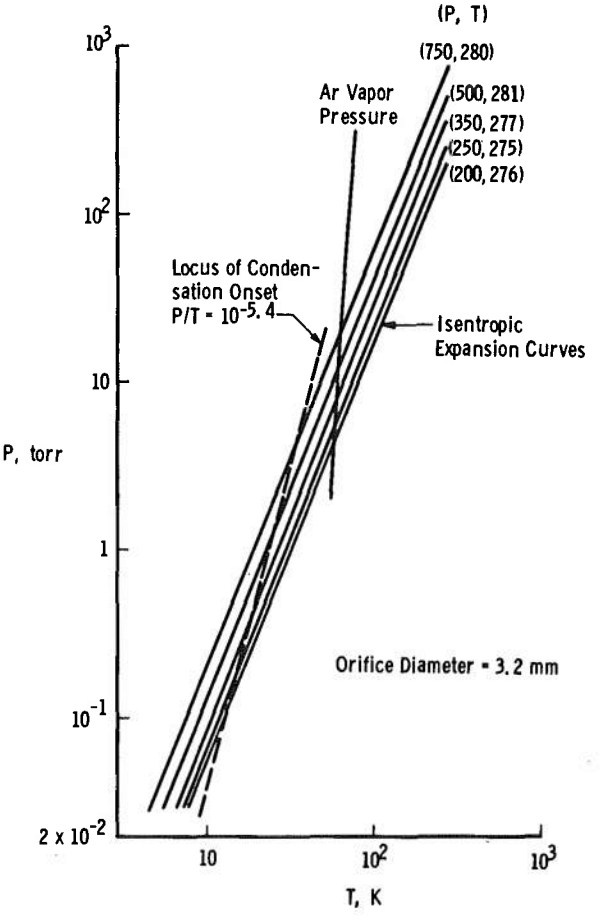

Figure 3. Condensation diagram of argon for a sonic orifice expansion.

The experimental results are shown in Figs. 4 through 8, and Fig. 9 shows all results on a single graph. The scattering data were normalized at one position for each value of P_o. The axial position selected had to be sufficiently far from the source that flow development was fulfilled, and the equations of Ref. 12 were valid and yet sufficiently close to the source that saturation had not yet occurred. Also of consideration was the quality and reproducibility of the data at the point in question; i.e., it was obviously desirable to select the best data point available for the reference value. The positions selected for this normalization are indicated in Figs. 4 through 8. Figure 7 shows the results of two separate axial scans, and the scatter shown is indicative of the reproducibility of the data. It should be noted that the predictions of Sherman and Ashkenas for the axial dependence of $(N_1/N_o)^o$ are restricted to $x/D \geq 1$, and the experimental data shown for $x/D < 1$ are denoted explicitly. It is interesting to look more closely at the values of $(N_1/N_o)^o$ shown in Fig. 9 for the region $x/D < 1$ and consider the extrapolated

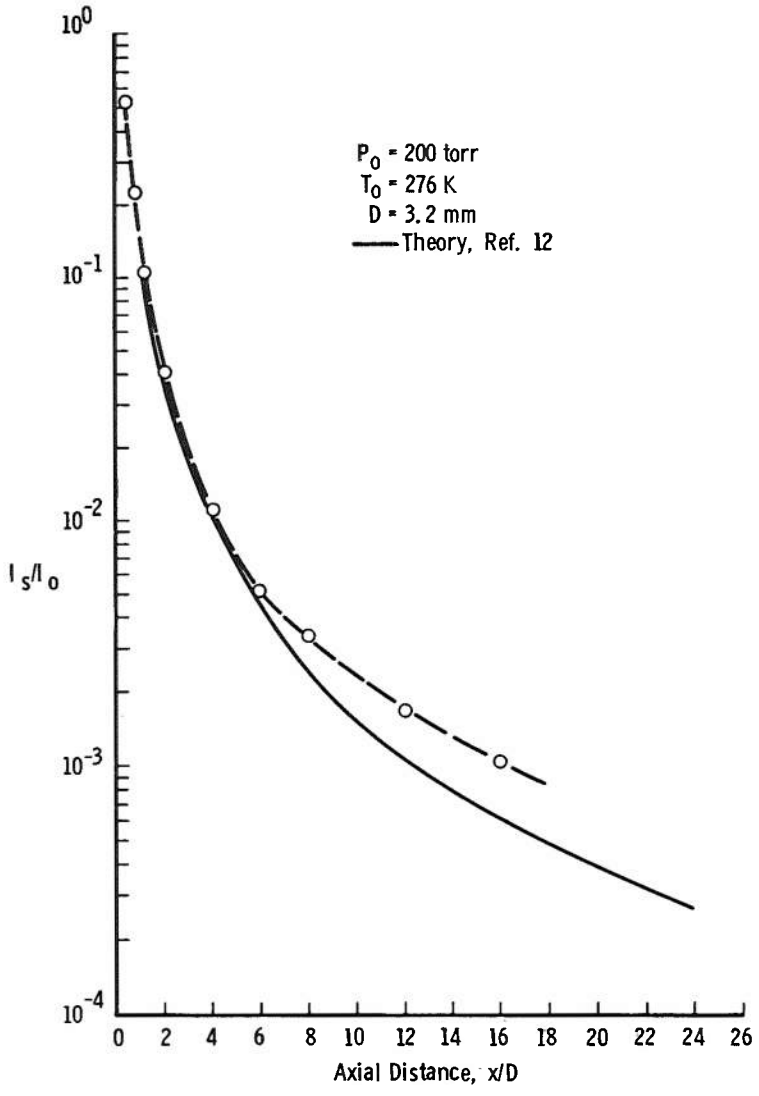

Figure 4. Rayleigh scattering results for P_o = 200 torr.

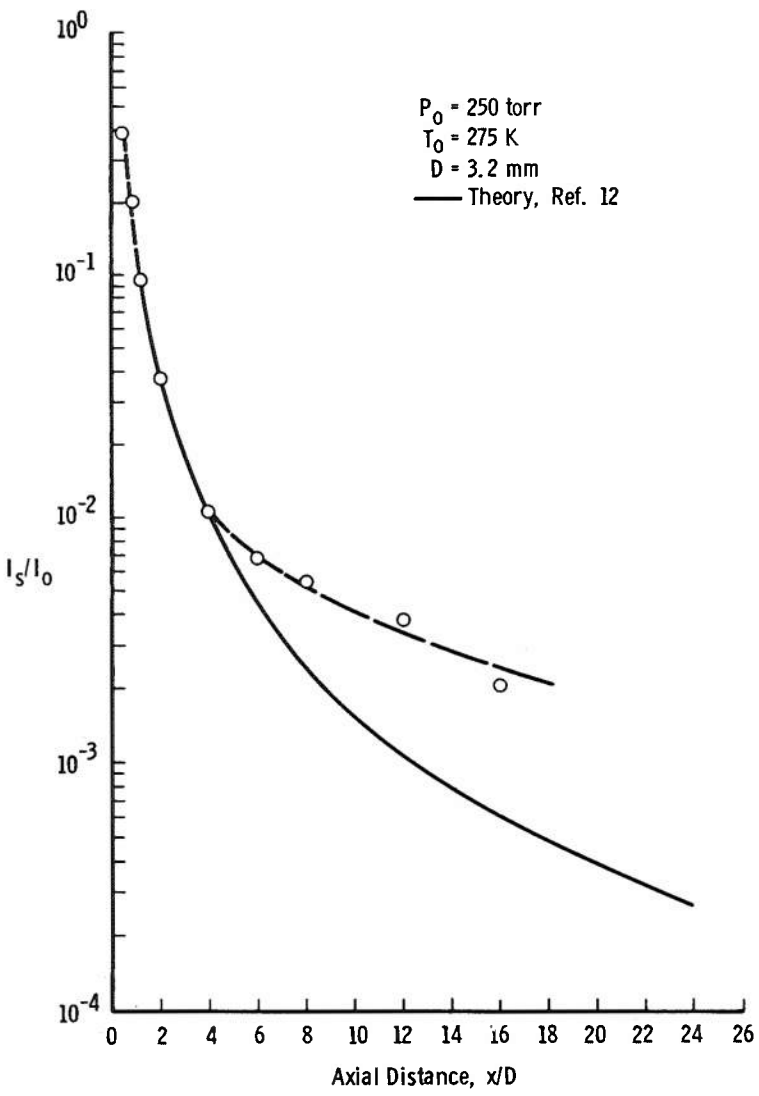

Figure 5. Rayleigh scattering results for P_o = 250 torr.

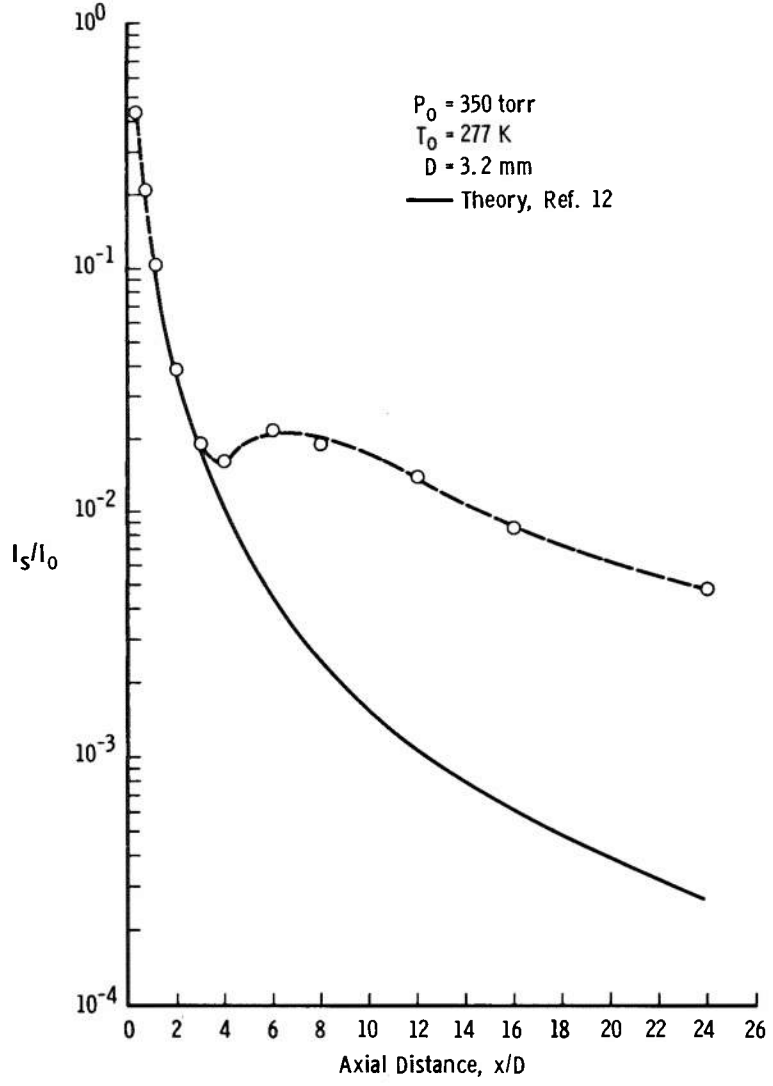

Figure 6. Rayleigh scattering results for P_o = 350 torr.

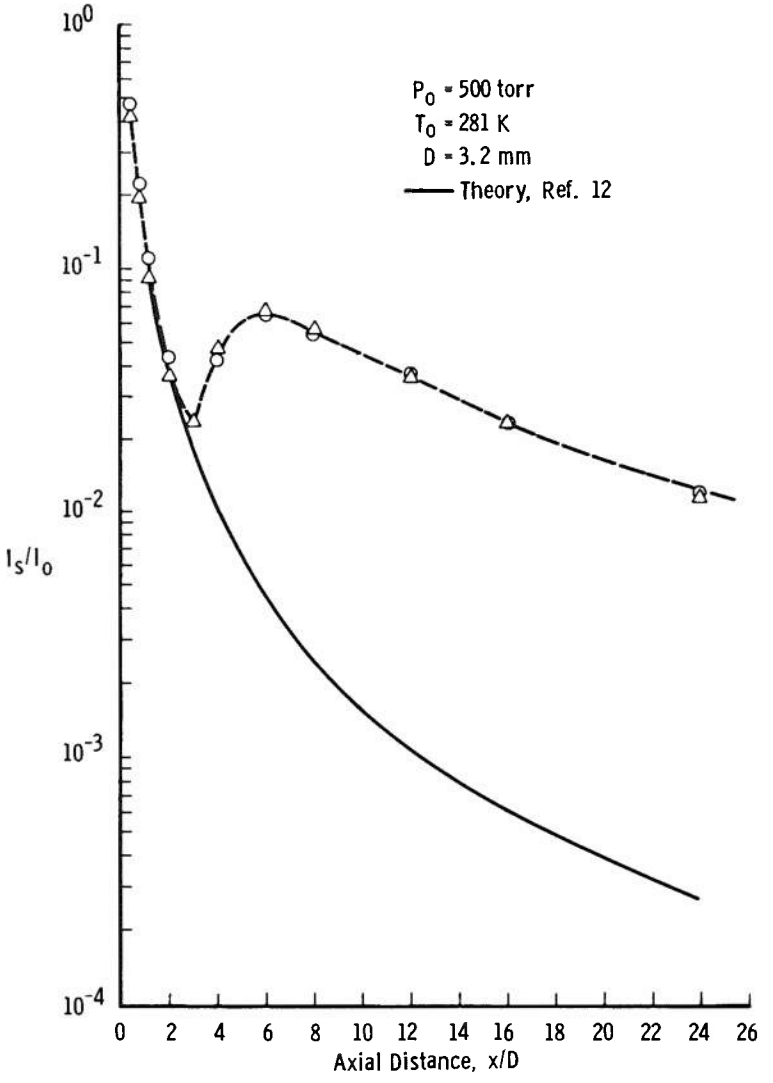

Figure 7. Rayleigh scattering results for P_o = 500 torr.

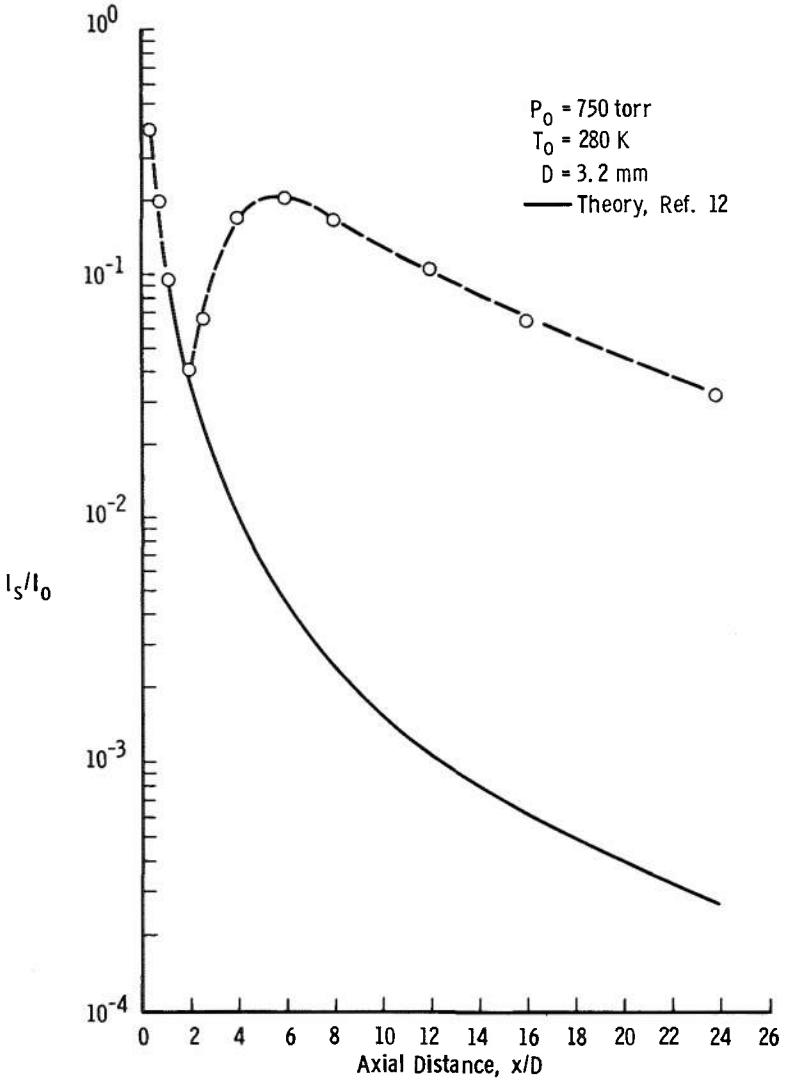

Figure 8. Rayleigh scattering results for P_o = 750 torr.

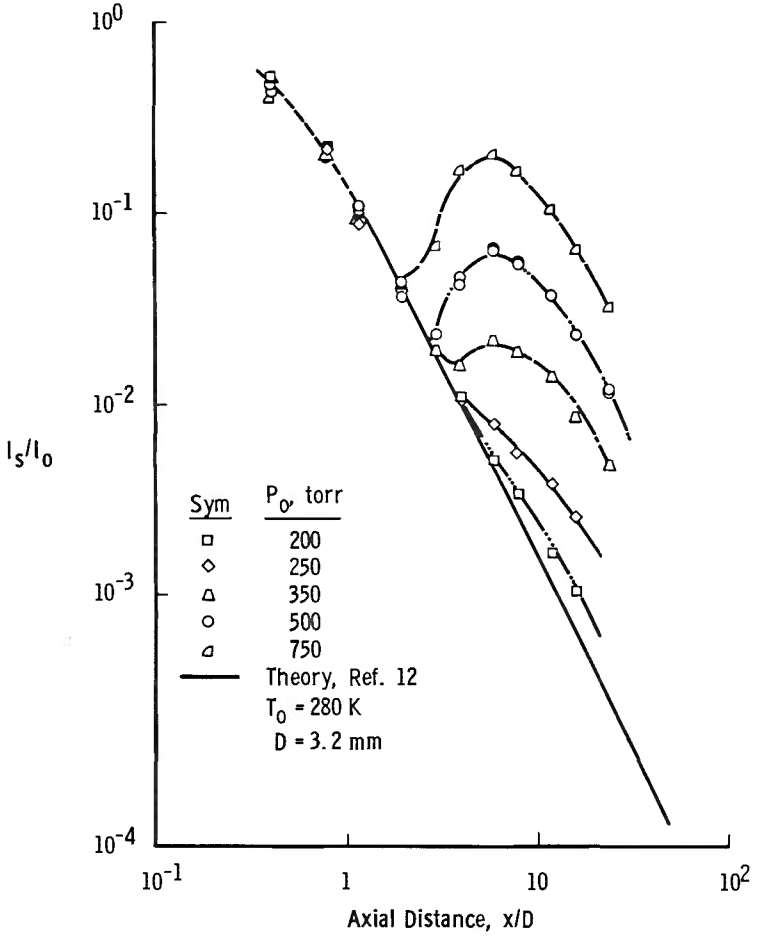

Figure 9. Axial variation of effective argon density $(N/N_o)_{eff}$.

value of the number density at $x/D = 0$. The initial reaction of this extrapolated value is that its value exceeds expectations. However, Ashkenas and Sherman present Mach number results of the transonic region for a sonic orifice flow of N_2 and show that at $x/D = 0$, the Mach number is approximately 0.70, not unity. This value of Mach number corresponds to an isentropic expansion area ratio of 1.0944. Therefore, assuming an identical area ratio at $x/D = 0$ for an Ar flow field, one finds the Mach number for Ar at $x/D = 0$ to be 0.69 as compared with 0.70 for N_2. Consequently, at $x/D = 0$ for Ar the calculated density ratio is approximately 0.68, and it is seen that the present experimental results are not inconsistent with this value. Moreover, for $\gamma = 5/3$, $(N_1/N_o)^o$ equals 0.487 at a Mach number of unity. It is seen from Fig. 9 that these present results indicate the development of sonic flow to occur at approximately $x/D = 0.40$. This result is pertinent for all kinetic rate models and calculations for which the spatial region $x/D < 1$ is of importance. As an example, in Ref. 2 calculations of the number of three-body collisions which occur in a sonic orifice flow field were performed. The assumption that $M = 1$ at $x/D = 0$ was made, and a functional form was assumed to connect $M = 1$ at $x/D = 0$ and $M = 2.81$ at $x/D = 1$. The present results give indication that the lower end-point of M is in error by approximately 30 percent, and it is noted that this error occurs in the higher density, higher collision frequency region of the expansion.

For the spatial region $1 \leq x/D \leq (x/D)_\theta$ it is seen that the agreement between experimental and predicted results is acceptable. The deviation of the measured values from the predicted density variation is accepted as a manifestation of the growth of molecular clusters and the onset of condensation. It is noted that for the lowest pressure observed, $P_o = 200$ torr, condensation resulted. This result is to be contrasted with the previous measurements (Ref. 6) of N_2 for which the isentropic behavior was verified over the axial region $1 \lesssim x/D \lesssim 25$ for $P_o = 500$ torr. The axial location of condensation onset $(x/D)_\theta$ is determined from Figs. 4 through 8, and the results are plotted in Fig. 10 as a function of P_o. From Fig. 10 it is seen that significant supersaturation is supported by Ar for P_o of approximately 200 to 250 torr, the flow having proceeded almost three orifice diameters beyond saturation before onset occurs. However, as P_o increases, $(x/D)_\theta$ decreases, and condensation follows closely on the heels of saturation for $P_o = 750$ torr. In fact, the results indicate that for reservoir pressures exceeding 750 torr, condensation can be expected to occur at saturation, i.e., the expansion can support no supersaturation whatsoever. The supersaturation ratio $s = P_S/P_\theta$, the ratio of saturation and onset pressures,

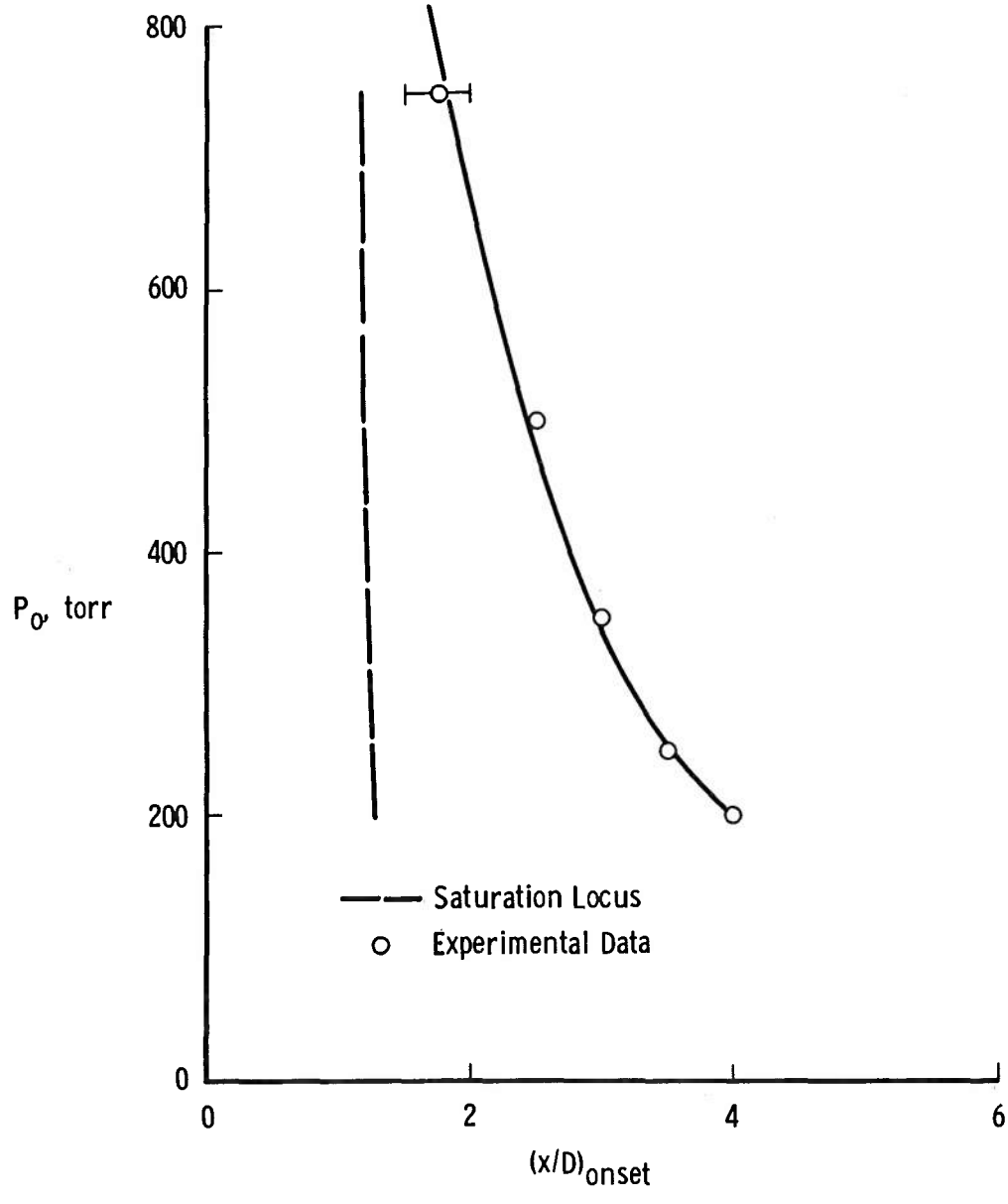

Figure 10. Pressure variation of condensation onset location of argon.

is easily obtained using the isentropic predictions of Ref. 12 and the results of Fig. 10, and s is shown as a function of P_o in Fig. 11. The experimentally observed degrees of supercooling, $T_S - T_\theta$, is shown versus reservoir pressures in Fig. 12. The locus of the onset of condensation in the P-T plane is shown by the dashed line in Fig. 3, and it was found that for the pressure range investigated this locus was approximately defined by the relation

$$P/T \approx 10^{-5.4}$$

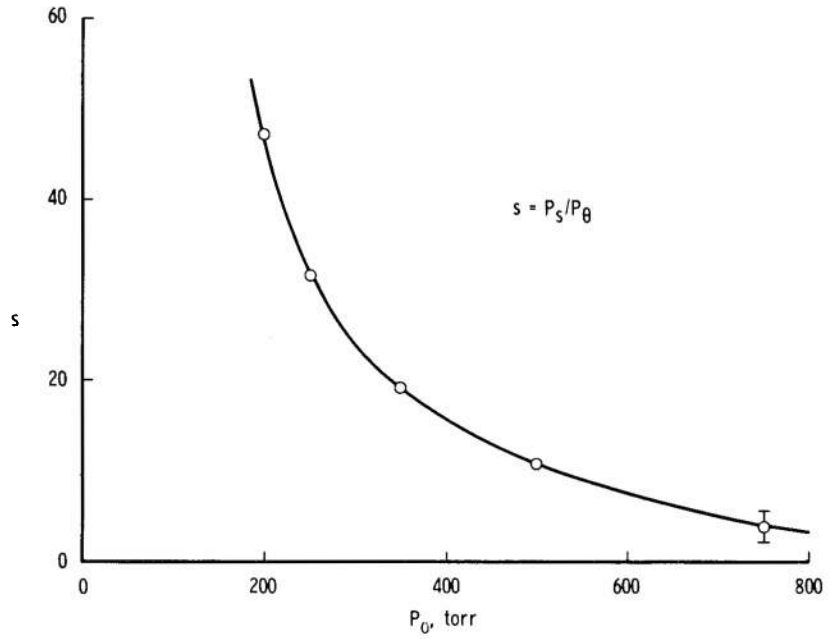

Figure 11. Pressure variation of supersaturation ratio.

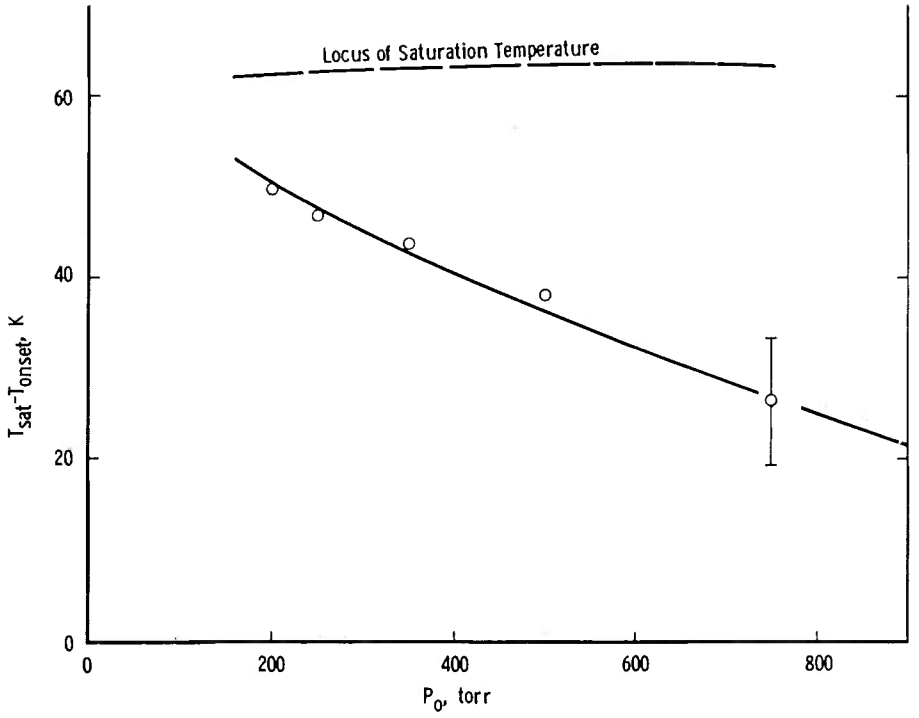

Figure 12. Pressure variation of degrees of supercooling.

Figure 13 shows the axial variation of the depolarization ratio, ρ, for P_o = 750 torr, and it is noted that ρ is defined as the ratio of perpendicular-to-parallel polarization intensity components; i.e.,

$$\rho = I_{s\perp}/I_{s\parallel}$$

It is seen by comparison of Figs. 13 and 8 that the axial region of ρ measurements includes the initial isentropic portion of the expansion as well as those of condensation onset and cluster growth.

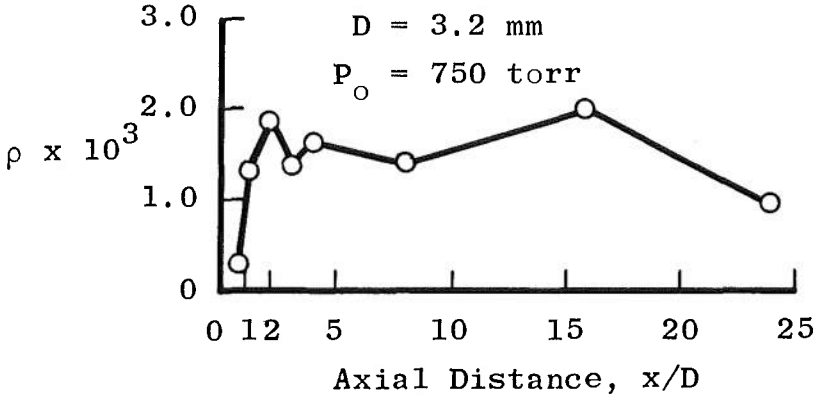

Figure 13. Axial variation of depolarization ratio of argon.

3.2 ANALYSIS

The results of Figs. 4 through 8 are used with Eq. (6) to determine the axial variation of the ratio R, and Fig. 14 shows the result for the five reservoir pressures investigated. It should be noted that for x/D = 24 the scattering signal for P_o = 200 torr is approximately 100 percent larger than its isentropic value, and for P_o = 750 torr a two-order-of-magnitude increase in I_s/I_o is observed. Of further interest is the steepening of the growth curve as P_o increases.

It is appropriate to consider in detail at this point the argon results of Golomb et al. (Ref. 2), and, in particular, focus our attention on Fig. 6 of this reference. It was found in this work that the dimer peak results scaled according to P_o^2D. Table 1 presents the P_o values of the present

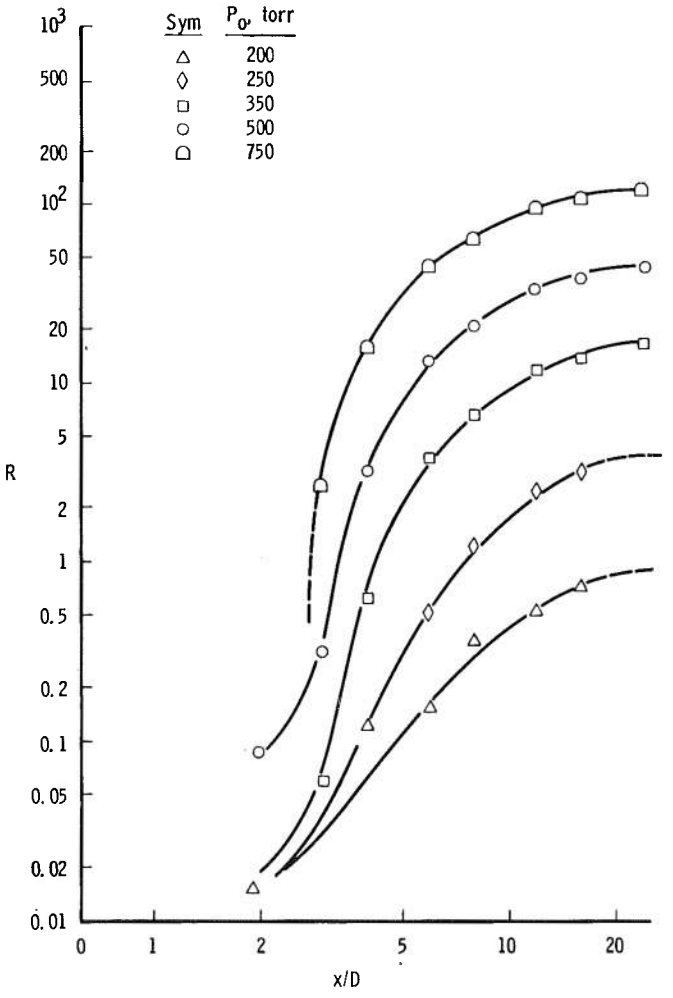

Figure 14. Axial variation of ratio R.

Table 1. Condensate Mass Fraction Results

P_o, torr	200	250	350	500	750
P_o (Refs. 2 and 5), torr	576	734	1008	1440	2159
u_c/u^o (Ref. 5)	1.001	1.007	1.020	1.033	1.077
g (Ref. 5)	≤0.001	0.015	0.042	0.07	0.16
$(N/Z)^*$ (Ref. 8)	20	30	55	100	200
g (this work)	0.046	0.13	0.23	0.30	0.37
X_c (this work) x 10^3	2.4	4.8	5.5	4.4	2.9

investigation, the corresponding P_o values of Ref. 2, as well as the velocity augmentation and condensation mass fraction of Ar observed by Bailey (Ref. 5) using the same apparatus but in a later work. For the 200-torr Rayleigh scattering results of Figs. 4 and 14, it is seen that at the reservoir pressure of 576 torr, corresponding to the orifice diameter 0.39 mm of Refs. 2 and 5, the dimer concentration is predominant, and the mass fraction of condensate is on the order of 0.1 percent or less. Assuming the 200-torr results of Fig. 14 to be the result of dimer scattering only, Eq. (8) yields a dimer mole fraction of approximately 0.25 and a condensate mass fraction of approximately 0.40, which differs by approximately three orders of magnitude from Bailey's results. If one attempts to take account of the obviously existent trimers shown in Fig. 6 of Ref. 2, it is found that $X_2/X_3 \approx 6.7$ from that figure. It is easily seen that Eq. (6) can be written as

$$R \approx X_2(\alpha_2/\alpha_1)^2 + (X_3/X_2)(\alpha_3/\alpha_1)^2$$

where, in view of the small value of g reported by Ref. 2 for this reservoir condition, the approximation

$$N_1^o \approx N_1 \approx N_T$$

is expected to be quite accurate. Assuming $\alpha_i/\alpha_1 \approx i$ and solving the above equation for X_2, using Eq. (9), one finds

$$g \approx 0.32$$

In view of the discrepancy of orders of magnitude for this reservoir condition, the inclusion of the trimers is not significant. Note that the results of Refs. 2 and 4 were acquired at $x/D > 500$, whereas those of Fig. 14 span the range of $1 < x/D < 25$. It must be concluded that the present results indicate scattering from clusters much larger in size than either dimers or trimers. The discrepancy between this conclusion and the results of Fig. 6 of Ref. 2 can be explained either by invoking a difficult-to-accept evaporation process of the cluster between $x/D = 25$ and 500 or that the mass spectrometric results previously discussed quite possibly are the manifestation of fragmentation processes of larger clusters.

The results of Hagena and Obert (Ref. 8) are now considered, and it is desired to obtain the predicted mean value $(N/Z)^*$ appropriate to our values of P_o and D. Reference 8 states that $(N/Z)^*$ for Ar scales

approximately as $P_o D^{0.8}$, and Fig. 15 shows the approximate results of Ref. 8 for the variation of $(N/Z)^*$ with P_o for two values of D.

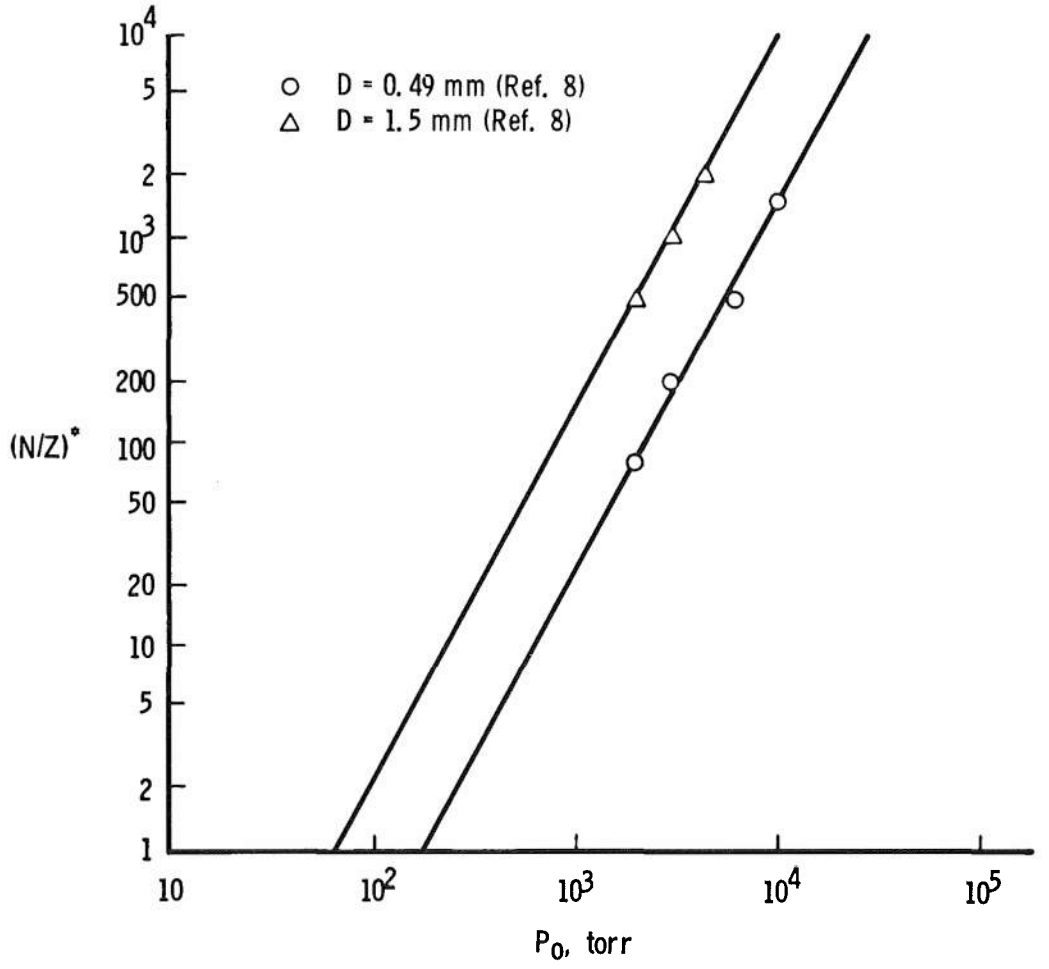

Figure 15. Variation of (N/Z)* with P_o.

Figure 16 shows the scaled results of Ref. 8 for a 3.2-mm orifice. It is seen that Hagena and Obert predict $(N/Z)^* = 20$ at $P_o = 200$ torr, D = 3.2 mm, and these values are listed in Table 1. Acknowledging both the distribution of cluster sizes encountered by Hagena and Obert and the absence of any better assumption, the authors assumed a Poisson distribution in cluster sizes with mean value $J = (N/Z)^*$ It should be noted that the value of $(N/Z)^*$ is not the mean value even if the distribution were Poisson; rather, it is such a value that one-half the ion cluster current is caused by cluster sizes $N/Z > (N/Z)^*$. Therefore, in principle one should plot the cumulative Poisson distribution functions

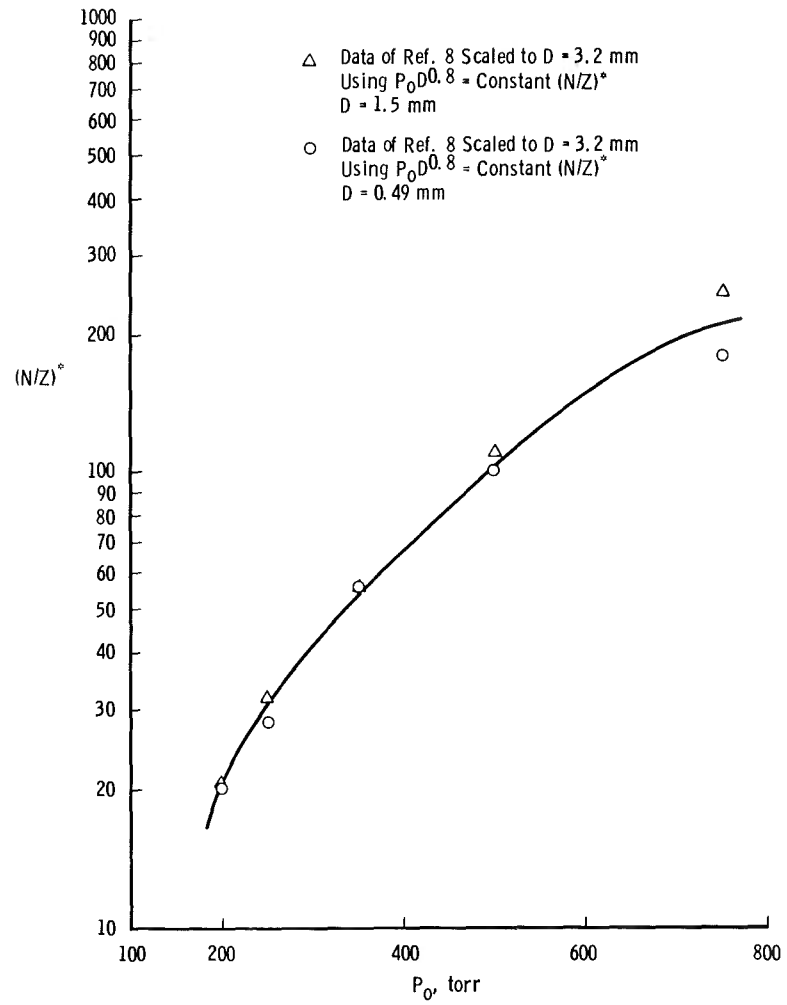

Figure 16. Scaled variation of (N/Z)* with P_o.

for various values of J and graphically determine the best value of J consistent with $(N/Z)^*$. The Poisson distribution function of J = 20 is shown in Fig. 17. $(N/Z)^*$ and J differ by approximately two percent, and this difference is henceforth neglected. Also, it should be noted that for J = 20, $p(1) < 10^{-4}$ and is negligible, as previously asserted. Using Eqs. (19) and (21) with the ascertained values of R and the values of $(N/Z)^* = J$ from Ref. 8, the mole and mass fraction of condensate X_c and g, respectively, are calculated, and comparisons are made with the results of Ref. 5. These results are shown in Table 1. It is seen that the g results differ from those of Bailey by over an order of magnitude for $P_o \leq 250$ torr, but the agreement improves to within a factor of 2 to 3 for the highest pressure. This higher pressure

discrepancy is perhaps quite acceptable considering the crudity of the model and approximations required for interpretation of Rayleigh scattering from clusters of unknown polarizabilities.

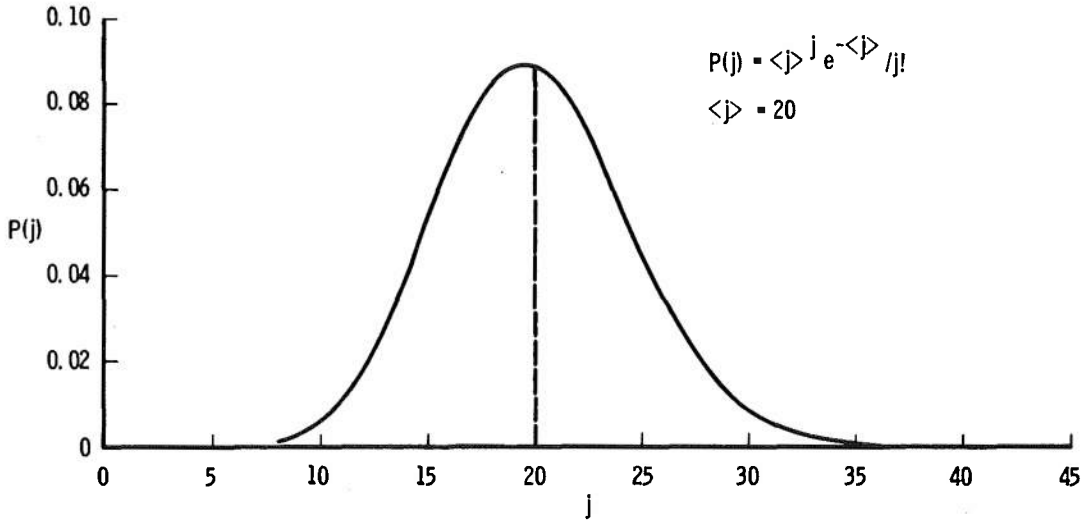

Figure 17. Poisson distribution function for a mean value of 20.

An alternate approach is to assume the validity of the values of g of Ref. 5 and to calculate J from the experimental values of R. Table 2 shows these results and those of Ref. 8 for comparison. Once again, very large values of cluster size are required for explanation of the Rayleigh results. However, the variation of J with P_o is somewhat peculiar, and the procedure employed for Table 1 calculations is preferred. Figure 18 shows the results for the variation of g with P_o. The discrepancy in mass fractions obtained by Ref. 5 and those provided by Rayleigh scattering for the low values of P_o is not understood. Although it is possible that the scattering data are anomalously high for P_o = 200 torr, if $(N/Z)^*$ = J is on the order of 20, one intuitively would expect values of g to be larger than 0.1 percent, but Bailey reports them to be less. It is noted that the flow speed is a measure of the

Table 2. Cluster Size Results Using Mass Fraction of Ref. 5.

P_o, torr	200	250	350	500	750
g (Ref. 5)	≤0.001	0.015	0.042	0.07	0.16
J	1000	300	390	590	610

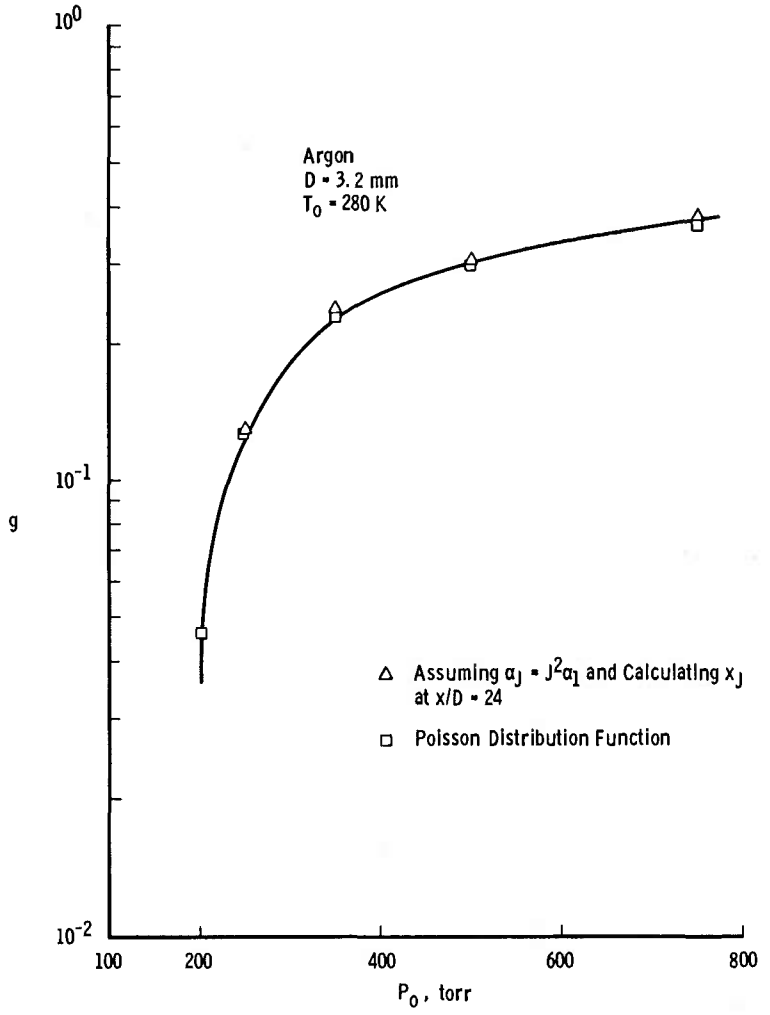

Figure 18. Variation of mass fraction g with reservoir pressure P_o.

mass fraction of condensate so long as certain conditions are fulfilled. and these conditions include negligible contributions to the enthalpy from both the translational and the internal modes of energy of both phases of matter. Whether violation of these conditions is the cause of at least part of the discrepancy is only speculation at this time.

Turning attention to the validity of the approximations made concerning the polarizability α_i of the i-mer, viz. $\alpha_i/\alpha_1 = i$, this assumption was made as a result of ignorance of the behavior of α of a cluster. Obviously the absence of interaction of atoms within the cluster is assumed, or, in other words, the effect of the polarization of the surrounding medium is neglected when calculating the electric field at an atomic

site. For the case of a dimer the estimate is reasonably good. Recent work of Levine (Ref. 14) has provided an approximate correction to the assumption $\alpha_2/\alpha_1 = 2$ which amounts to only three parts per hundred.

The experimental results for the depolarization ratio ρ shown in Fig. 13 are seen to increase from a value of approximately 3×10^{-4} at $x/D = 1$, reach an initial maximum value on the order of 2×10^{-3} at approximately $x/D = 2$, and finally decrease to 1×10^{-3} at $x/D = 25$. As discussed previously, an increase in ρ from its negligible value for the monomer Ar manifests the existence of clusters. It is, of course, of interest to compare the experimental results with theoretical predictions. Levine and Birnbaum (Ref. 15) have considered the problem of the calculation for Ar_2 of the polarizability asymmetry factor β, which is defined in terms of the longitudinal, α_L, and transverse, α_T, polarizabilities of the body axes of the cylindrically symmetrical molecule as

$$\beta = \alpha_L - \alpha_T$$

They assumed the interatomic potential of Ar_2 to be given by the Lennard-Jones 12-6 potential, and they found an expression for β as a function of the interatomic separation. Assuming their nondimensionalized distance of separation to be on the order of unity, for the purpose of order of magnitude calculation, the expression of Ref. 16 for β gives $\beta = 0.2$. Using the expression (Ref. 11)

$$\rho_2 = 3\beta^2 / (45\alpha^2 + 3\beta^2)$$

one finds

$$\rho_2 \approx 2.6 \times 10^{-4}$$

It is seen that the experimental value of ρ at $x/D = 1$ is 2.9×10^{-4} and increases upon obvious further cluster growth as one proceeds downstream. The rather good agreement between the measured and predicted values of the depolarization ratio near $(x/D)_\theta$ makes it appear quite likely that dimers are observed during the earliest part of the cluster growth process but that larger clusters rapidly assume the predominant cluster specie role and do so by $x/D \doteq 2$ at the latest. Since ρ is independent of density in the first approximation, the observed variation of the depolarization ratio with axial distance is a clear indication of a changing cluster symmetry and cluster number. Referring to Fig. 13, it is seen that if the dimer region is restricted to $x/D \lesssim 2$,

as evidenced by the ρ data, the dimer mole fraction X_2 must be approximately less than or equal to 0.025. Consequently, the experimental results for P_o = 750 torr appear to place a maximum value for X_2 of 0.025 on the proposed theoretical descriptions.

Regarding comparisons of the present results with other investigations, particularly those of Yealland et al. (Ref. 10), it was not possible to accurately employ the functional relations given by Ref. 10 because the P_o and D values employed in the present study lie far outside the range of validity of that work.

Finally, concerning the electron diffraction results of Ref. 4, the orifice diameter was 0.2 mm and the experimental data for P_o of 2.5 to 3.0 atm at room temperature indicated a short-range order of the scatterer, implying a liquid phase or dimers for Ar. If one assumes P_o^2D scaling, the pressure value corresponding to a D = 3 mm is approximately 500 torr, at which P_o the Rayleigh scattering results are consistent with cluster sizes on the order of 100. This result is an example of the limitation of diffraction data; assuming short-range ordering, or a quasi-liquid phase, information concerning the size of the cluster is absent. It should be noted that the smaller orifice of Audit required higher values of P_o than employed in the present work using a 3-mm orifice to obtain equivalent condensate results. However, the expansions from the higher values of P_o of Audit resulted in the flow saturating in the liquid phase regime rather than the solid phase, as in the present case. The exact nature of the variations to be expected as a result of this difference in source conditions is not understood at this time. Finally, for utilization of the diffraction technique for quantitative interpretation of cluster densities, more work appears to be required to enable the correlation of scattered electron intensity and specific cluster concentrations.

4.0 DISCUSSION AND CONCLUSIONS

The Rayleigh scattering measurements reported herein have demonstrated the utility of this technique for locating condensation onset in a sonic orifice expansion of argon. Additionally, this location provides information concerning the supersaturation ratio as a function of reservoir pressure. Cluster growth is also observed, but, of course, the data are ambiguous in the sense that the cluster number density and polarizability are inseparable without additional information. Three

types of additional information were employed and compared for consistency with our results: (1) mass spectrometric detection of individual clusters, (2) time-of-flight measurements of the monomer flow speed, and (3) a charge-normalized mean cluster size using a retarding potential technique. This comparison, as has been mentioned preiously, required the use of the so-called scaling law relating some characteristic of the condensation process to the reservoir pressure and orifice source diameter. It was found that the Rayleigh scattering data were irreconcilible with the assumption of quantitative accuracy of mass spectrometric cluster signals of Ref. 2; this result was not shocking since the difficulties of faithfully sampling such a flow are well known. However, it was found that the assumption of validity of the cluster sizes reported by Hagena and Obert (Ref. 8) did enable the calculation of reasonable values of condensate mole and mass fractions. These values of mass fraction were in order-of-magnitude agreement as obtained using flow speed measurements, except for the lowest pressures investigated. For these no quantitative explanation is offered. Additionally, the measurement of the depolarization ratio, ρ, of the argon clusters through the cluster growth region provides a rather interesting demonstration of the spatial symmetry changes which occur during the accretion process. Moreover, the order-of-magnitude agreement between the measured and predicted values of ρ over a finite axial distance appears to delimit the existence region of the dimer in the direction of the flow and, thereby, imposes an additional condition which must be fulfilled by any proposed theoretical description of the condensation process.

For the purpose of extracting as much information as possible from the Rayleigh scattering data, the present authors have resorted to two assumptions which are worthy of note, not because of a desire to champion their validity, but, rather, because they do affect the conclusions. First, a Poisson distribution function was assumed to characterize the cluster size distribution. Although such an assumed distribution is admittedly crude, it is evidently superior to a Dirac delta function description, and for small mean cluster sizes the Poisson distribution might be expected to be reasonable. Second, the polarizability of an i-mer has been assumed to be i times that of the monomer. The basis for this assumption is the very weak binding of the clusters, a feature which will help to maintain the independence of the atomic species and thereby insure additivity of the polarizability. This approximation is obviously quite good for van der Waal's dimers, but its accuracy for increasingly larger clusters is uncertain. However, despite any inaccuracy inherent in our treatment, an inescapable conclusion is

the caution which must be exercised in attempting to fit various kinetic rate models to mass spectrometric dimer signals of condensing expansion flow fields, such as has been done by Milne et al. (Ref. 3). The same conclusion obviously does not apply to the molecular, or effusion, source work of Leckenby and Robbins (Ref. 7), because, quite simply, the dimers were produced by equilibrium processes in the reservoir, the molecular beam was formed without collisions, and the possibility of fragmentation effects in the mass spectrometer are minimal.

Further work is in progress which is designed to explore the various scaling laws relating reservoir parameters and involving other gaseous species. For molecular species, rotational Raman scattering measurements have been performed through the condensation onset region, and it is hoped that such information will provide additional insight for the understanding of two-phase flow fields.

REFERENCES

1. Golomb, D., Good, R. E. and Brown, R. F. "Dimers and Clusters in Free Jets of Argon and Nitric Oxide." The Journal of Chemical Physics, Vol. 52, No. 3, February 1970, pp. 1545-1551.

2. Golomb, D., Good, R. E., Bailey, A. B., Busby, M. R., and Dawbarn, R. "Dimers, Clusters and Condensation in Free Jets, II." The Journal of Chemical Physics, Vol. 57, No. 9, November 1972, pp. 3844-3852.

3. Milne, Thomas A., Vandegrift, A. Eugene, and Greene, Frank T. "Mass-Spectrometric Observations of Argon Clusters in Nozzle Beams, II. The Kinetics of Dimer Growth." The Journal of Chemical Physics, Vol. 52, No. 3, February 1970, pp. 1552-1560.

4. Audit, P. "Liaisons Intermolécularies dans les Jets Supersoniques Etude par Diffraction d'Electrons." Jour. Physique, Vol. 30, 1969, pp. 192-202.

5. Bailey, A. B. "Effects of Condensation on Gas Velocity in a Free-Jet Expansion." AEDC-TR-73-93 (AD 762503), June 1973.

6. Lewis, J. W. L., Williams, W. D., Price, L. L. and Powell, H. M. "Nitrogen Condensation in a Sonic Orifice Expansion Flow." AEDC-TR-74-36, July 1974.

7. Leckenby, R. E. and Robbins, E. J. "The Observation of Double Molecules in Gases." Proceedings of the Royal Society of London, Vol. 291, 1966, pp. 389-412.

8. Hagena, O. F. and Obert, W. "Cluster Formation in Expanding Supersonic Jets: Effect of Pressure, Temperature, Nozzle Size, and Test Gas." The Journal of Chemical Physics, Vol. 56, No. 5, March 1972, pp. 1793-1802.

9. Obert, W. "Multiple Ionization of Rare Gas Clusters by Electron Impact." International Journal of Mass Spectrometry and Ion Physics, Vol. 9, August 1972, pp. 295-297.

10. Yealland, R. M., Deckers, J. M., Scott, I. D. and Touri, C. T. "Dimer Concentrations in Supersonic Free Jets." Canadian Journal of Physics, Vol. 50, October 1972, pp. 2464-2470.

11. Hirschfelder, Joseph O., Curtiss, Charles F. and Bird, R. Byron Molecular Theory of Gases and Liquids, John Wiley and Sons, New York, 1954.

12. Ashkenas, H. and Sherman, F. S. "The Structure and Utilization of Supersonic Free Jets in Low Density Wind Tunnels," Rarefied Gas Dynamics. Edited by J. H. de Leeuw, Fourth Symposium, Vol. II, Academic Press, New York, 1966, pp. 84-105.

13. Hilsenrath, J., Beckett, C. W., Benedict, W. S., Fano, L., Hoge, H. J., Masi, J. F., Nuttall, R. L., Touloukian, Y. S., and Woolley, H. W. Tables of Thermal Properties of Gases. National Bureau of Standards Circular 564, Washington, D.C., November 1955.

14. Levine, Howard B. "Spectroscopy of Dimers," Journal of Chemical Physics. Vol. 56, No. 5, March 1972, pp. 2455-2473.

15. Levine, Howard B. and Birnbaum, George "Determination of Models for Collision-Induced Polarizability by the Method of Moments." The Journal of Chemical Physics, Vol. 55, No. 6, September 1971, pp. 2914-2917.

NOMENCLATURE

D	Orifice diameter
g	Condensate mass fraction
I_O	Incident laser beam intensity
I_S	Scattered laser beam intensity
$I_{S\parallel}$, $I_{S\perp}$	Parallel and perpendicular polarization components of I_S
K_α	Optical calibration constant for Eq. (1)
N	Number density
N_i	Number density of i-mer
N/Z	Number-to-charge ratio for cluster
$(N/Z)^*$	Mean number-to-charge ratio for distribution of clusters
P	Pressure
$p(i)$	Probability of observing i-mer among all clusters
R	Scattered intensity ratio defined by Eq. (6)
s	Supersaturation ratio
T	Temperature
T_R	Rotational temperature
u	Flow speed
X	Mole fraction
X_i	Mole fraction of i-mer
x	Axial distance
α	Polarizability of molecule
α_i	Polarizability of i-mer
α_L, α_T	Longitudinal and transverse components of α
β	Molecular asymmetry parameter
Δu	Change in u attributable to condensation
γ	Specific heat ratio

λ	Wavelength
ρ	Depolarization ratio

SUBSCRIPTS

c	Variable evaluated for condensing flow
S	Saturation value
T	Total value
o	Reservoir value
θ	Condensation onset value

SUPERSCRIPT

o	Isentropic value

CGS units used unless otherwise stated.